MARTIN MARIETTA ENERGY SYSTEMS LIBRARIES

3 4456 0279553 5

ORNL/TM-10556

ornl

OAK RIDGE
NATIONAL
LABORATORY

MARTIN MARIETTA

Neutral and Plasma Shielding Model for Pellet Ablation

W. A. Houlberg
S. L. Milora
S. E. Attenberger

LIBRARY LOAN COPY
DO NOT TRANSFER TO ANOTHER PERSON

OPERATED BY
MARTIN MARIETTA ENERGY SYSTEMS, INC.
FOR THE UNITED STATES
DEPARTMENT OF ENERGY

Printed in the United States of America. Available from
National Technical Information Service
U.S. Department of Commerce
5285 Port Royal Road, Springfield, Virginia 22161
NTIS price codes—Printed Copy: A03; Microfiche A01

This report was prepared as an account of work sponsored by an agency of the United States Government. Neither the United States Government nor any agency thereof, nor any of their employees, makes any warranty, express or implied, or assumes any legal liability or responsibility for the accuracy, completeness, or usefulness of any information, apparatus, product, or process disclosed, or represents that its use would not infringe privately owned rights. Reference herein to any specific commercial product, process, or service by trade name, trademark, manufacturer, or otherwise, does not necessarily constitute or imply its endorsement, recommendation, or favoring by the United States Government or any agency thereof. The views and opinions of authors expressed herein do not necessarily state or reflect those of the United States Government or any agency thereof.

ORNL/TM-10556
Dist. Category UC-20 g

Fusion Energy Division

NEUTRAL AND PLASMA SHIELDING MODEL FOR PELLET ABLATION

W. A. Houlberg
S. L. Milora
S. E. Attenberger
Computing and Telecommunications Division
Martin Marietta Energy Systems, Inc.

DATE PUBLISHED — October 1987

Prepared by the
OAK RIDGE NATIONAL LABORATORY
Oak Ridge, Tennessee 37831
operated by
MARTIN MARIETTA ENERGY SYSTEMS, INC.
for the
U.S. DEPARTMENT OF ENERGY
under contract DE-AC05-84OR21400

MARTIN MARIETTA ENERGY SYSTEMS LIBRARIES
3 4456 0279553 5

CONTENTS

ACKNOWLEDGMENT v

ABSTRACT vii

1 INTRODUCTION 1

2 THE NEUTRAL SHIELD 3

3 THE COLD PLASMA SHIELD 7

4 ELECTRON AND FAST ION DISTRIBUTIONS 11

5 SELF-LIMITING ABLATION IN THE COLLISIONLESS LIMIT . . . 15

6 SOLUTION TECHNIQUE 17

7 DISCUSSION 19

8 SUMMARY 29

REFERENCES 31

ACKNOWLEDGMENT

Development and refinement of the various features of this model have progressed intermittently over a period of several years. Without the support of experimental groups on ISX, PDX, Alcator-C, PLT, D-III, TFTR, and JET, without the pellet ablation data provided by those groups, and without their patience in applying developmental versions of the PELLET code, this work would not have been possible. One of the authors (WAH) would particularly like to thank M. L. Watkins and the JET experimental team for providing the opportunity to finally complete and rigorously test the model on an extensive data base during his assignment to the JET project in 1986.

This research was sponsored by the Office of Fusion Energy, U. S. Department of Energy, under contract DE-AC05-84OR21400 with Martin Marietta Energy Systems, Inc.

ABSTRACT

The neutral gas shielding model for ablation of frozen hydrogenic pellets is extended to include the effects of (1) an initial Maxwellian distribution of incident electron energies; (2) a cold plasma shield outside the neutral shield and extended along the magnetic field; (3) energetic neutral beam ions and alpha particles; and (4) self-limiting electron ablation in the collisionless plasma limit. Including the full electron distribution increases ablation, but adding the cold ionized shield reduces ablation; the net effect is a modest reduction in pellet penetration compared with the monoenergetic electron neutral shielding model with no plasma shield. Unlike electrons, fast ions can enter the neutral shield directly without passing through the cold ionized shield because their gyro-orbits are typically larger than the diameter of the cold plasma tube. Fast alpha particles should not enhance the ablation rate unless their population exceeds that expected from local classical thermalization. Fast beam ions, however, may enhance ablation in the plasma periphery if their population is high enough. Self-limiting ablation in the collisionless limit leads to a temporary distortion of the original plasma electron Maxwellian distribution function through preferential depopulation of the higher-energy electrons.

1 INTRODUCTION

Injection of hydrogenic pellets has become increasingly popular as a means of fueling, modifying density profiles, probing plasma behavior, and, in many cases, improving confinement properties of toroidal plasmas. Understanding the pellet ablation process is helpful for understanding present experiments and is crucial for planning new experiments and determining pellet injector technology requirements. The penetration of hydrogenic pellets in tokamak experiments has substantially confirmed the neutral gas shielding model for pellet ablation [1,2]. However, because many simplifying physical and computational assumptions have been made in computer adaptations of the model, serious questions have remained about the accuracy of predictions concerning pellet penetration in higher-temperature, lower-collisionality plasmas. Enhanced ablation by fast ions from auxiliary heating or by fast alphas from deuterium-tritium (D-T) fusion reactions is also an effect that needs to be quantified.

The Parks-Turnbull-Foster [3] and Milora-Foster [4] neutral shielding models have been the most widely used models for pellet ablation calculations. Both models evaluate the shielding effect of a cold dense layer of gas surrounding the pellet. The former model is more complete in that it uses a full treatment of the hydrodynamic equations for the gas shield. The distinguishing feature of the Milora-Foster model is the use of an empirical relationship between the electron energy flux incident on the neutral shield and the line-integrated neutral density in the shield. This empirical relationship was obtained from full solutions to the hydrodynamic equations for spherical expansion of the neutral gas under conditions of uniform volumetric heating by the incident electrons. Detailed information about the radial structure of the neutral gas shield is sacrificed for computational efficiency, but the net pellet ablation rate is the same. Both models assume only incident electrons with a monoenergetic distribution to simplify the evaluation of the energy flux to the pellet surface from the electron-stopping cross sections in neutral hydrogen gas.

Milora [5] proposed extending the Milora-Foster model by including energy fluxes from fast ions and alphas in the empirical relationship for the neutral cloud solution and evaluating the additional energy fluxes to the pellet surface from hydrogen and alpha-stopping cross sections in the neutral shield. The results were at least in qualitative agreement with ISX-B observations of enhanced ablation during neutral beam injection heating [6]. Nakamura et al. [7] used Milora's arguments for including fast ions to extend the Parks-Turnbull-Foster treatment of the hydrodynamic equations. They found that the uniform heating approximation is valid except when the range of electrons in the neutral cloud is much shorter than that of the fast ions while the incident energy fluxes are comparable ($T_e \leq 1\,\mathrm{keV}$), that is, when a large amount of the electron energy is deposited on the surace of the neutral cloud. This nonuniform heating, however, may be attributable in part to treating the incident electron and ion distributions as monoenergetic; a full treatment of these distribution functions would tend to smear out the heating.

None of these models takes into account the enhanced shielding that occurs when the ablatant becomes ionized and constrained to flow in a tube along the magnetic field. Kaufmann et al. [8] used a single-velocity, two-temperature, partially ionized, compressible, ideal-gas approximation to describe the flow of ionized ablatant along the magnetic field lines. The critical element in the model is in obtaining the flow of electron energy through the ionized ablatant. A conduction model was used that treated ablatant electrons and plasma electrons as a single, continuous fluid. This resulted in very effective shielding with ablation rates reduced by an order of magnitude from the the neutral shielding rates. For

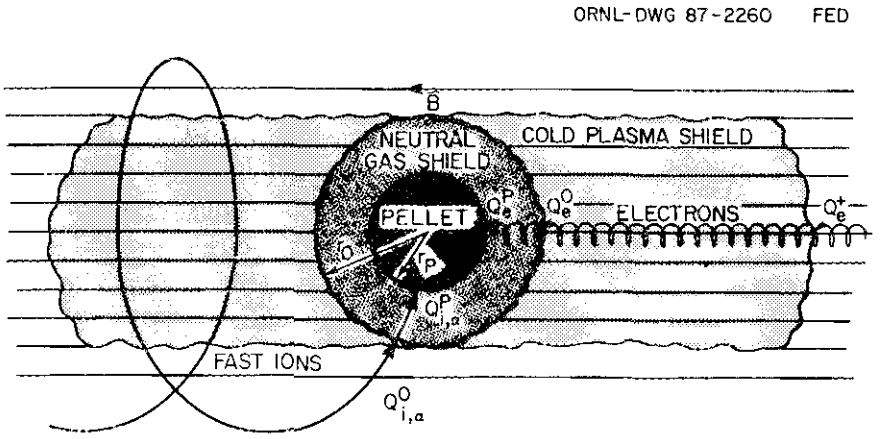

Figure 1: Schematic illustration of the pellet ablation process showing the neutral and cold plasma shields. Electrons are constrained by the magnetic field and therefore must penetrate both the ionized and neutral shields. Fast ions with their large gyroradii may directly enter the neutral cloud normal to the magnetic field.

the single electron fluid conduction model to be valid, the collision mean-free path must be much shorter than the temperature gradient scale length, a condition that the authors admit is violated.

Our work uses the Milora-Foster neutral shielding model as a starting point (i.e., we use the uniform heating approximation for neutral shield solution). We extend the treatment of incident plasma electrons from a monoenergetic distribution to a multiple energy group formulation, and we include fast ions in a similar way. This multigroup treatment of the incident plasma distribution functions allows incorporation of "self-limiting" ablation in the collisionless plasma limit. By self-limiting ablation we mean any reduction in ablation caused by a finite plasma; the electron-electron collision timescale in the plasma is typically longer than the time for a pellet to cross a magnetic surface, so a collisionless model is appropriate for present experiments. Once the neutral gas becomes ionized, it is constrained to flow along the magnetic field, increasing the shielding for incident electrons, as illustrated in Fig. 1. The inclusion of the plasma shield is similar to the treatment by Kaufmann et al. [8], except that we model the flow of electron energy through the ionized and neutral shields in a convective energy flux limit rather than a conductive (Spitzer-Härm) limit. These physics enhancements are made to the neutral shielding model while still maintaining a computationally efficient model for analyzing experimental results.

The basic equations governing the neutral shield are reviewed in Section 2 and then expanded in Section 3 to include a cold plasma shield extending along the magnetic field. The plasma electron and fast ion distributions are presented in Section 4, and the relevant timescales for depletion of energetic particles for self-limiting ablation in the collisionless limit are evaluated in Section 5. Computational techniques for solving the extended set of equations are given in Section 6, and the effects of various physical extensions of the model are evaluated in Section 7.

2 THE NEUTRAL SHIELD

The set of equations governing the ablation of a solid hydrogenic pellet and the establishment of a dense neutral gas shield surrounding the pellet includes an energy balance at the pellet surface (assumed to be spherical for computational simplicity even though it is typically a cylinder of nominally equal length and diameter) [3,4]

$$\left(\frac{\lambda_s^m}{2}\right)\dot{N} = -\lambda_s^m n_s^m (4\pi r_p^2)\dot{r}_p = 4\pi r_p^2 \bar{Q}^p \tag{1}$$

where λ_s^m is the molecular heat of sublimation, $\dot{N}$ is the atomic ablation rate at the pellet surface, n_s^m is the molecular density of the solid, r_p is the pellet radius, and $\bar{Q}^p$ is the effective energy flux averaged over the pellet surface. All energy reaching the pellet surface is assumed to result in ablation rather than bulk heating of the pellet; this may not be the case for very energetic particles (e.g., runaway electrons). The molecular densities of solid (H_2, D_2, T_2) are $(2.63,\ 2.98,\ 3.15) \times 10^{28}\,\mathrm{m}^{-3}$, and the heats of sublimation are $(10.7,\ 15.2,\ 17.5) \times 10^{-6}\,\mathrm{keV}$ at their respective triple points [9]. The solution is not sensitive to λ_s^m when it is much smaller than the energy of the incident plasma electrons [4]; throughout this work, $\lambda_s^m = 10^{-5}\,\mathrm{keV}$.

Hydrodynamic solutions of the neutral cloud expansion involve mass, momentum, and energy balances. A fit to the solution obtained for uniform heating by electrons in the neutral cloud is given by [4]

$$\dot{r}_p = -1.25\frac{\int_{r_p}^{r_o} n^o dl}{2 r_p n_s^m}\left[q^o r_p \frac{(\gamma-1)}{2}\right]^{1/3} \tag{2}$$

where q^o is the net energy flux normalized to the line-integrated density in the neutral cloud,

$$q^o \equiv \frac{(\bar{Q}^o - \bar{Q}^p)}{2A_p m_p \int_{r_p}^{r_o} n^o dl} \tag{3}$$

$\gamma = 7/5$ is the ratio of specific heats for hydrogen gas, m_p is the mass of a proton, A_p is the atomic mass number of the pellet species, $\bar{Q}^o$ is the incident energy flux averaged over the surface of the neutral cloud, n^o is the atomic density in the neutral cloud, r_o is the radius of the neutral cloud, and the integral represents the line-integrated density of the neutral cloud. All units are in mks except temperatures and energies, which are in keV except where the Boltzmann constant k is used to imply that kT is in joules.

Equations (1) and (2) can be combined to eliminate $\dot{r}_p$, leaving a single equation involving $\bar{Q}^p$, $\bar{Q}^o$, and $\int_{r_p}^{r_o} n^o dl$. The following analysis shows how $\bar{Q}^o$ is determined by the plasma conditions and how $\bar{Q}^p$ is related to $\bar{Q}^o$ through $\int_{r_p}^{r_o} n^o dl$ to complete the set of equations.

First, consider incident particles of arbitrary energy (the distribution of incident energies is discussed in Section 4). Consider the energetic electrons and ions from the plasma to be test particles that are degraded in energy by collisions with the target. The stopping cross section, σ, is defined such that

$$\frac{dE}{dl} = -n\sigma \tag{4}$$

where n is the target density, l is the path length, and E is the test particle energy.

For electrons above a critical energy, $E_e^* \approx 0.1\,\mathrm{keV}$, a fit to experimental measurements of the stopping cross section in molecular hydrogen is given by [4]

$$\sigma_e^o = \frac{1}{a_{e1} + a_{e2}E_e}\,\mathrm{m}^2\,\mathrm{keV/electron} \tag{5}$$

where $a_{e1} = 4.7 \times 10^{21}$ and $a_{e2} = 8.0 \times 10^{21}$. A term that is important only below 0.1 keV has been dropped from the expression of Ref. [4] to permit an analytic solution for the energy of an electron at the pellet surface in terms of its energy at the neutral cloud surface. Substituting Eq. (5) into Eq. (4) and integrating with the boundary conditions $E_e(r_o) = E_e^o$ and $E_e(r_p) = E_e^p$ gives

$$a_{e1}(E_e^o - E_e^p) + \frac{a_{e2}}{2}(E_e^{o2} - E_e^{p2}) = \int_{r_p}^{r_o} n^o dl \tag{6}$$

which can be solved for E_e^p in terms of the initial energy and line-integrated density in the neutral cloud,

$$E_e^p = -\frac{a_{e1}}{a_{e2}} + \sqrt{\left(\frac{a_{e1}}{a_{e2}} + E_e^o\right)^2 - \frac{2}{a_{e2}} \int_{r_p}^{r_o} n^o dl} \tag{7}$$

Equation (7) is valid up to a line-integrated density that reduces E_e^p below E_e^*

$$\int_{r_p}^{r_o} n^o dl \leq \int_{r_*}^{r_o} n^o dl = a_{e1}(E_e^o - E_e^*) + \frac{a_{e2}}{2}(E_e^{o2} - E_e^{*2}) \tag{8}$$

The total energy flux in this convective flow regime is proportional to the particle energy and the incident particle flux (which is constant in steady state to avoid particle accumulation); thus,

$$\bar{Q}_e^p = \frac{E_e^p}{E_e^o}\bar{Q}_e^o \tag{9}$$

If the line-integrated density of the neutral cloud is greater than the critical value, the electrons enter the elastic scattering regime, and the energy flux at the pellet surface is given by [10,5]

$$\bar{Q}_e^p = \bar{Q}_e^* \frac{C+1}{C + \exp[\alpha_e(\int_{r_p}^{r_o} n^o dl - \int_{r_*}^{r_o} n^o dl)/2]} \tag{10}$$

$$\bar{Q}_e^* = \bar{Q}_e^o \frac{E_e^*}{E_e^o} \tag{11}$$

where $\alpha_e = 1.8 \times 10^{-20}\,\mathrm{m}^2/\mathrm{molecule}$ is the elastic scattering coefficient and C is a constant of order unity; we use $C = 2$.

An effective stopping cross section in the elastic scattering regime can be defined from Eq. (10) with $r_p \to r$

$$\sigma_e^o = \frac{E_e}{n^o \bar{Q}_e}\frac{d\bar{Q}_e}{dr} \tag{12}$$

The stopping cross sections of Eqs. (5) and (12) are shown in Fig. 2; the fits for the two regimes cross at 0.075 keV, but we use 0.1 keV for the transition.

If plasma ions are ignored in the ablation process, electrons are taken as monoenergetic, and there is no additional shielding by a cold, dense plasma outside the neutral cloud, the ablation problem is fully specified and equations can be solved directly [4]. The incident energy for a Maxwellian distribution is $E_e^o = 3T_e/2$, and the effective one-sided energy flux incident on the neutral cloud is

$$\bar{Q}_e^o = \frac{Q_e}{2} = \frac{1}{2}\frac{4}{3}\left(\frac{n_e \bar{v}_e}{4} E_e^o\right) = \frac{n_e T_e}{4}\left(\frac{8kT_e}{\pi m_e}\right)^{1/2} \tag{13}$$

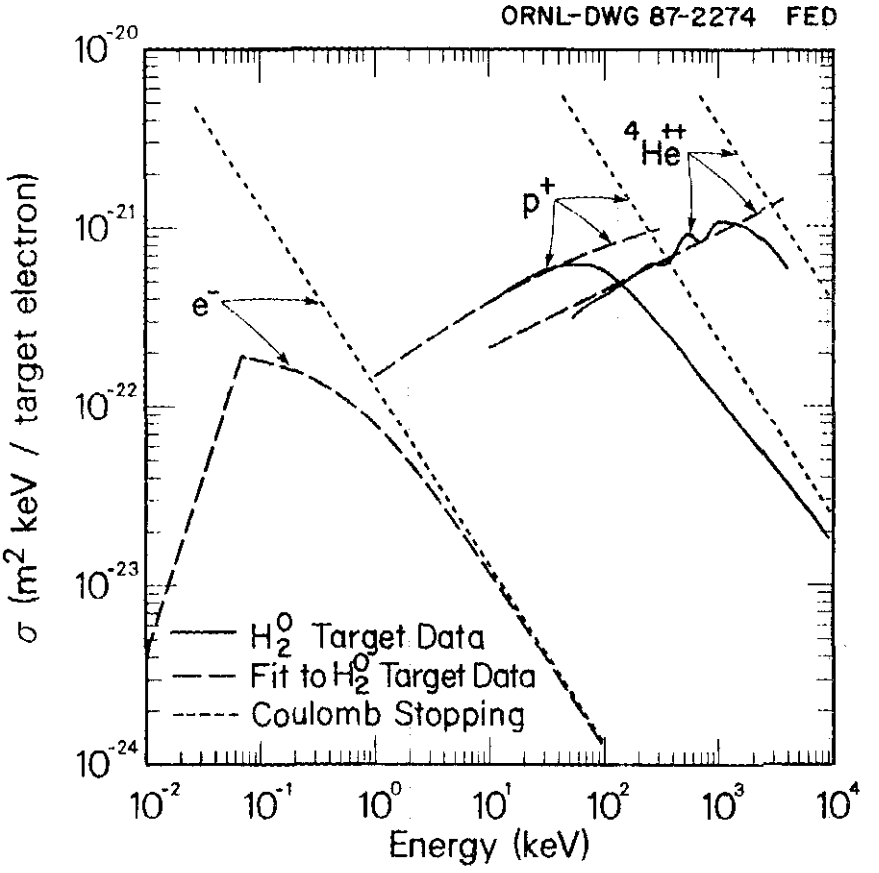

Figure 2: Stopping cross sections for electrons, hydrogenic ions, and helium ions. Solid curves represent experimental data for stopping in hydrogen gas, long-dashed curves are fits to the experimental data, and short-dashed curves are theoretical values for Coulomb stopping in a cold electron plasma.

where the factor of 2 for the effective flux arises from the fact that electrons are constrained to flow along the magnetic field lines; the surface area normal to the electron flow is only half of the total surface area of the neutral cloud. The incident particle and energy fluxes of thermal ions are much smaller than the incident electron fluxes, so their effect is negligible.

Milora has extended the neutral shielding model by summing the fast ion and electron energy fluxes [5]

$$\bar{Q} = \bar{Q}_e + \bar{Q}_i + \bar{Q}_\alpha \tag{14}$$

where contributions from fast alphas have also been included.

The stopping cross section for hydrogenic ions in neutral hydrogen [11] can be approximated by

$$\sigma_i^o \approx \frac{1}{a_{i1}/\sqrt{E_h} + a_{i2}} \, \mathrm{m}^2\,\mathrm{keV/atom} \tag{15}$$

where $a_{i1} = 61.86 \times 10^{20}$, $a_{i2} = 6.658 \times 10^{20}$, and $E_h = E_i/A_i\,\mathrm{keV}$ is the energy per nucleon of the energetic ion. Both the data of Ref. [11] and the fit of Eq. (15) are shown in Fig. 2. The fit is valid in the range of $10 < E_h < 60\,\mathrm{keV}$, which is appropriate for most current neutral beam injection experiments. Above 60 keV per nucleon, the fitted cross section is too large and underestimates the effect of beam ions. Below 10 keV per nucleon, no data are available, but the cross section should scale as $\sqrt{E_h}$ as in the fitted expression. Integrating Eq. (4) over the cross section given in Eq. (15) and then solving for E_i^p in terms of E_i^o and the line-integrated density of the neutral cloud yields

$$E_i^p = b^2(-1 + \sqrt{1+c})^2 \tag{16}$$

$$c \equiv \frac{2\sqrt{E_i^o}}{b} + \frac{(E_i^o - \int_{r_p}^{r_o} n^o dl/a_{i2})}{b^2}$$

$$b \equiv \frac{a_{i1}\sqrt{A_i}}{a_{i2}}$$

The stopping cross section for energetic helium in neutral hydrogen [11] is approximated by

$$\sigma_\alpha^o = a_{\alpha 1}(E_{\mathrm{He}^4})^{a_{\alpha 2}} \, \mathrm{m}^2\,\mathrm{keV/atom} \tag{17}$$

where $a_{\alpha 1} = 1.01 \times 10^{-22}$, $a_{\alpha 2} = 0.325$, and $E_{\mathrm{He}^4} = E_\alpha(4/A_\alpha)\,\mathrm{keV}$ is the effective energy for He^4 so the expression is applicable to energetic He^3 in minority ion cyclotron resonance heating (ICRH) experiments. The range data of Ref. [11] are converted to a stopping cross section by $1/\sigma = n(dR/dE)$ with the derivative evaluated from a spline fit to the range data. Figure 2 shows both the data (the oscillations are due to differentiation of the data) and the fit of Eq. (17). The fit is valid in the range $50\,\mathrm{keV} < E_{\mathrm{He}^4} < 2\,\mathrm{MeV}$. Above 2 MeV the fitted cross section is too large and therefore overestimates the effectiveness of the neutral shield. Substituting Eq. (17) into Eq. (4) and integrating gives

$$E_\alpha^p = \left[E_\alpha^{o(1-a_{\alpha 2})} - (1-a_{\alpha 2})a_{\alpha 1}\int_{r_p}^{r_o} n^o dl\right]^{1/(1-a_{\alpha 2})} \tag{18}$$

The expressions for σ_i^o and σ_α^o have been chosen such that Eq. (4) can be integrated and then solved analytically for the energy at the pellet surface in terms of the energy incident on the cloud. In extending the range of the fits, it would be desirable—from a computational standpoint—to maintain this analytic relationship.

3 THE COLD PLASMA SHIELD

Once the ablated hydrogen becomes ionized, it is constrained to flow along the magnetic field lines where it offers additional shielding. In the case of electrons (whose gyro-orbits are much smaller than the pellet and therefore closely follow the field lines), this additional shielding can be important. We first derive an expression for the line-integrated density in the cold plasma tube. Then, we treat the plasma electrons and fast ions as test particles incident on the cold plasma target, use the free-streaming limit for the test particle current, and use Coulomb scattering to reduce the energy of the incident particles.

Assume that the ablatant makes a transition from nominally spherical flow to flow along the magnetic field at the effective ionization radius r_o. In steady state (on the timescale of the neutral cloud formation), the rate of ablation at the pellet surface, $\dot{N}$, is equal to the outgoing plasma flux times the cross-sectional area of the tube

$$\dot{N} = n^+ v(2\pi r_o^2) \tag{19}$$

where v is the streaming velocity of the cold plasma, n^+ is its density, and the factor of 2 arises from the flow in both directions away from the pellet. Taking a tube with a constant cross section, using $v = dl/dt$, and integrating over time and distance along the tube yields an expression for the line-integrated density of the cold, dense plasma,

$$\int_{r_o}^{\infty} n^+ dl = \frac{\dot{N}}{\pi r_o v_p} \tag{20}$$

where v_p is the pellet velocity, and the time required for the neutral cloud to cross a flux surface,

$$\tau_{po} = \frac{2r_o}{v_p} \tag{21}$$

has been used for the time interval.

Converting the expression for energy relaxation by Coulomb scattering on a cold target to a stopping cross section gives

$$\sigma_{ab} = 10^{-6} \left(\frac{m_a}{m_b}\right) \frac{2\pi e^2 Z_a^2 Z_b^2 \lambda_{ab}}{E_a (4\pi\epsilon_o)^2} \,\mathrm{m}^2\,\mathrm{keV/particle} \tag{22}$$

where a denotes the incident energetic particles, b is the target particles, and λ_{ab} is the Coulomb logarithm. The subscripts a and b apply to either ions or electrons. From the mass dependence, it can be seen that the cold electrons in the outflowing cold plasma are primarily responsible for the energy degradation of the incident ions and electrons. When $\lambda_{ab} \approx 10$ is used, the Coulomb stopping cross sections match onto the experimental values of stopping cross sections for electrons, hydrogenic ions, and alphas at very high energies, as shown in Fig. 2. In other words, at high enough incident particle energies, it does not matter whether the electrons in the target are free or bound—Coulomb relaxation predominates.

The Coulomb stopping cross section can be used in Eq. (4) to obtain analytic expressions for the energies of electrons, fast ions, and alphas entering the neutral cloud along the magnetic field lines in terms of their energies in the bulk plasma. Letting $\sigma_{ab} = C_{ab}/E_a$ gives

$$E_a^{o2} = E_a{}^2 - 2C_{ab} \int_{r_o}^{\infty} n^+ dl \tag{23}$$

where E_a is the energy incident on the ionized cloud and E_a^o is the energy incident on the neutral cloud. The Coulomb stopping cross sections for ions and alphas in the energy ranges of interest are larger than the neutral stopping cross sections by at least an order of magnitude; thus, even a modest ionized cloud can be very effective at stopping energetic particles from entering along the magnetic field. However, the gyro-orbits of fast ions and alphas are much larger than the ionization radius so they can directly enter the neutral cloud normal to the magnetic field. Thus, it is possible to approximate the effective fast ion and alpha energy fluxes to the neutral cloud as

$$\bar{Q}_{i,\alpha}^o = \frac{Q_{i,\alpha}}{2} \tag{24}$$

where the factor of 2 arises from considering the component of the one-sided flux normal to the magnetic field lines. The particle flux of hot electrons is assumed to be constant along the magnetic field so that

$$\bar{Q}_e^o = \frac{Q_e^+}{2}\frac{E_e^o}{E_e} \tag{25}$$

where the factor of 2 in this case comes from the constraint that electrons enter only along the field lines. The energy flux incident on the cold plasma, $\bar{Q}_e^+$, is the one-sided energy flux in the unperturbed plasma unless finite plasma corrections (self-limiting ablation) are required; this is discussed further in Section 5.

Equations (20) and (23)–(25) allow us to obtain values of the fluxes incident on the neutral cloud in terms of the external plasma parameters if the effective neutral cloud radius is known. The ionization radius can be obtained from a full solution of the hydrodynamic equations with the appropriate atomic physics included, but that is beyond the level of the current model. A simpler alternative is to apply a macroscopic energy balance on the neutral cloud, matching the incident energy flux over the surface to the power required to ionize the ablatant

$$\dot{N}\,E_{\rm ion} = \bar{Q}^o 4\pi r_o^2 \tag{26}$$

We have not been successful in obtaining a stable computational scheme that gives reliable results when this equation is included; the solution tends to collapse toward $r_o = 0$ where a very small level of ablation supports a large line density in a narrow, cold plasma tube. Clearly, a constraint is needed to maintain the effective ionization radius greater than the pellet radius.

Other alternatives are to use the results of a more complete model for cloud expansion that includes the requisite atomic physics for evaluating the effective ionization radius or to use direct experimental measurements of the ionization radius. Kaufmann et al. [8] used the empirical approximation $r_o \approx 2.5 r_p$ drawn from the critical radius of Parks [12], which gives $r_o \approx 5\,\mathrm{mm}$ for ASDEX pellet injection conditions. Calculations were performed over the range of $1.7 \lesssim r_o < 5.6\,\mathrm{mm}$. Holographic interferometry of pellets in ISX-B showed strong discontinuities in the electron density preceding and following the pellet (normal to the magnetic field) at a distance of 0.1–0.2 mm from the pellet surface [13]. The discontinuity was interpreted as being caused by a $\vec{J} \times \vec{B}$ force limiting the cross-field expansion and indicates significant ionization. The free electron density in the region of high neutral hydrogen density also appeared to be anomalously high. Measurements of H_α and H_β emission on PLT by McNeill et al. [14] were interpreted as indicating an emission volume of $\approx 1.8\,\mathrm{cm}^3$. Assuming a spherical expansion, this leads to a spherical shell of $r_o \approx 2\,\mathrm{cm}$ and thickness $\approx 0.36\,\mathrm{mm}$. Similar measurements by the TFR Group [15] along with the

observation of thin striations along the magnetic field lines were interpreted as indicating that the transition from spherical expansion to flow along the field lines occurs at a much smaller radius. Separation of well-resolved striations of ≈ 7 mm indicate that the radius of transition from spherical to parallel flow could be no more than a few millimeters.

We have used two empirical models for the ionization radius: fixing the ionization radius and fixing the thickness of the neutral shield. From preliminary tests of the model against JET data [16,17] and noting the variability of pellet size (from experiment to experiment and also during the ablation process itself), the option of a fixed thickness is preferable,

$$r_o = r_p + \Delta_o \tag{27}$$

4 ELECTRON AND FAST ION DISTRIBUTIONS

The plasma electrons are assumed to have a Maxwellian distribution at the ambient density and temperature before the pellet is injected. The one-sided energy flux for a Maxwellian is given by

$$Q_e = \frac{4}{3} J_e E_e \tag{28}$$

where $E_e = 3T_e/2$ is the average electron energy, $J_e = n_e \bar{v}_e/4$ is the random particle flux integrated over one side of the distribution, and $\bar{v}_e = (8kT_e/\pi m_e)^{1/2}$ is the mean velocity. Now break up the distribution into energy groups. Let $x \equiv v/v_{te}$, where $v_{te} \equiv (2kT_e/m_e)^{1/2}$; then the normalized density, average electron energy, and one-sided energy flux in the interval $x_{j+1} < x < x_j$ are

$$\hat{n}_{ej} = \frac{n_{ej}}{n_e} = \left[\frac{-2}{\sqrt{\pi}} x e^{-x^2} + \mathrm{erf}(x)\right]\Bigg|_{x_{j+1}}^{x_j} \tag{29}$$

$$\hat{E}_{ej} = \frac{E_{ej}}{E_e} = \frac{1}{\hat{n}_{ej}}\left[-\frac{1}{3\sqrt{\pi}}(4x^3 + 6x)e^{-x^2} + \mathrm{erf}(x)\right]\Bigg|_{x_{j+1}}^{x_j} \tag{30}$$

$$\hat{Q}_{ej} = \frac{Q_{ej}}{Q_e} = -\left(1 + x^2 + \frac{x^4}{2}\right) e^{-x^2}\Bigg|_{x_{j+1}}^{x_j} \tag{31}$$

For N_e energy groups, the x_j can be chosen so that $\hat{Q}_{ej} = 1/N_e$ (i.e., each group has equal weight in the energy balance). These values of x_j can then be used to evaluate the energy weighting for each group, $\hat{E}_{ej}$, for use in the energy flux attenuation through the ionized and neutral clouds. The choice of one group reduces the model to the original monoenergetic electron model.

Under some operating conditions in tokamak experiments, nonthermal electron distributions lead to enhanced pellet ablation. Runaway electrons have been shown to be important in several experiments—the more detailed of these observations have been on ISX-B [6] and TFTR [18]. Lower hybrid wave heating experiments on Alcator-C have shown a large population of nonthermal electrons with tail temperatures in the range of 30–100 keV and have exhibited reduced pellet penetration [19]. It is possible to incorporate an additional class of electrons for modeling the effects of nonthermal electrons. However, a model for the energy and spatial distributions of these electrons is a nontrivial development; relativistic effects may become important in evaluating energy degradation by the cloud, and deep penetration to the pellet interior by a few very energetic electrons may result in bulk heating or pellet break-up rather than surface erosion. The runaway electron tail may not be relevant to pellet fueling of reactor plasmas, but non-ohmically driven current may lead to an enhanced electron tail that could be important in evaluating pellet penetration.

For fast hydrogenic ions and alpha particles, a set of energy group boundaries, E^b_{fj}, and the ion density in each energy interval, n_{fj}, are sufficient specifications along with the number of groups, N_f. This is compatible with information available in many plasma transport analysis codes from either a time-dependent or a steady-state solution of the Fokker-Planck equation. We present here an example of how the group structure and density can be set up for a steady-state approximation following the multigroup method of Ref. [20] for solving the slowing down problem; we use this procedure in evaluating the fast ion ablation rates in Section 7.

Let the total source strength of particles at energy E_{fo} be P_f watts integrated over the plasma. The source profile can be characterized by a profile shape factor $H_f(r)$, which is normalized to the total plasma volume, V_p, as

$$\frac{1}{V_p}\int_{V_p} H_f(r)dV = 1 \tag{32}$$

Then the population in the highest-energy group, allowing for charge-exchange loss of hydrogenic ions, is

$$n_{f1} = \frac{H_f(r)P_f}{1.602\times 10^{-16}E_{fo}V_p(\tau_{cx1}^{-1}+\tau_{fs1}^{-1})} \tag{33}$$

For lower-energy groups, the population depends on the thermalization loss from the higher-energy group, rather than on the initial source strength at E_{fo},

$$n_{fj} = \frac{n_{fj-1}}{\tau_{fsj-1}}\frac{1}{(\tau_{cxj}^{-1}+\tau_{fsj}^{-1})} \tag{34}$$

The group charge-exchange rate is determined by the background neutral hydrogen density, n_o, and the charge-exchange cross section evaluated at the velocity of the energetic fast hydrogen ion,

$$\tau_{cxj}^{-1} = n_o\langle\sigma v\rangle_{cxj} \tag{35}$$

The time needed to slow down through velocity interval j is

$$\tau_{fsj} = \frac{\tau_{fs}}{3}\ln\left[\frac{(v_{fj}^b)^3+v_c^3}{(v_{fj+1}^b)^3+v_c^3}\right] \tag{36}$$

where $v_{fj}^b = (2kE_{fj}^b/m_f)^{1/2}$ is the upper boundary of interval j and τ_{fs} is the energy relaxation time on electrons,

$$\tau_{fs}^{-1} = \frac{4}{3}\frac{\sqrt{2\pi m_e}}{m_f}\frac{Z_f^2e^4n_e\lambda_{fe}}{(4\pi\epsilon_o)^2}\frac{1}{(kT_e)^{3/2}} \tag{37}$$

v_c is the critical velocity at which energy relaxation on electrons and ions is equal,

$$v_c^3 = \frac{3\sqrt{\pi}}{4}\left(\frac{m_e}{m_p}\right)[Z]v_{te}^3 \tag{38}$$

and $[Z]$ is the effective charge for ion collisions,

$$[Z] = \frac{\sum_k n_kZ_k^2/A_k}{n_e} \tag{39}$$

where k is summed over thermal ion species.

The average energy and one-sided energy flux for a group are calculated from the group densities and energy boundaries assuming a steady-state distribution within each group in the absence of group sources or charge-exchange terms. The steady-state form of the distribution within a group is then

$$f_j(v) = \frac{C_{fj}}{v^3+v_c^3} \tag{40}$$

C_{fj} is determined by normalizing to the group density; that is,

$$C_{fj} = \frac{3n_{fj}}{4\pi \ln\left[\frac{(v^b_{fj})^3+v_c^3}{(v^b_{fj+1})^3+v_c^3}\right]} \tag{41}$$

and then the average energy and one-sided energy flux within a group are

$$E_{fj} = \frac{2\pi}{n_{fj}} \int_{v^b_{fj+1}}^{v^b_{fj}} m_f v^4 f_j(v) dv \tag{42}$$

$$Q_{fj} = \frac{\pi}{2} \int_{v^b_{fj+1}}^{v^b_{fj}} m_f v^5 f_j(v) dv \tag{43}$$

For a large enough number of groups, the energy could be more simply approximated by the mean of the group boundary values; a similar treatment could be used for the energy flux.

5 SELF-LIMITING ABLATION IN THE COLLISIONLESS LIMIT

Even though the time required for a pellet and its cloud to cross a flux surface is very short (typically $\tau_{po} \approx 5$--$10\ \mu$s), it is long enough, under some conditions, for the plasma electron distribution function far from the pellet to be significantly perturbed from its initial state. This perturbation results in a reduction in the particle and energy fluxes to the pellet cloud and therefore reduces pellet ablation. This "self-limiting" ablation was evident in early ISX-B experiments where the ablation rate took a severe dip as the pellet approached and crossed the magnetic axis [6], and it was speculated then that the major dips in the H_α signals away from the magnetic axis may be caused by rational flux surfaces.

Two timescales for the plasma electrons far from the pellet are relevant, the electron-electron collision time and the parallel flow time. If the flow time is shorter than τ_{po}, a significant fraction of the plasma electrons interact directly with the ablation cloud and a finite-plasma response must be considered in the ablation model. When the collision time is longer than τ_{po}, a collisionless response is appropriate for the plasma electrons. An adiabatic response of the plasma electrons has been used in earlier modeling efforts [21]; this consists of a continual mixing of the cold electrons generated by ionization of the pellet with the hot plasma electrons while keeping the energy content either constant or reduced by the energy required for ionization. The electron distribution is assumed to be Maxwellian at all times; thus, the model is appropriate for a collisional plasma. A collisionless response will be shown to be more relevant for current tokamak experiments.

For the electron-electron collision time, consider electrons above the thermal velocity of the initial Maxwellian distribution. These have the highest probability of reaching the pellet and penetrating the shield because of their higher energy and lower stopping cross section. The energy-scattering time for an electron of normalized energy $x \equiv v^2/v_{te}^2$ is

$$\tau_{ee}^E \approx \frac{(4\pi\epsilon_o)^2 m_e^2 v_{te}^3}{8\pi e^4 \lambda_{ee} n_e} x^{3/2} \tag{44}$$

when $x > 1$. For $T_e = 2\,\mathrm{keV}$, $n_e = 3 \times 10^{19}\,\mathrm{m}^{-3}$ (typical of current experiments), and $x = 2$, we obtain $\tau_{ee}^E \approx 75\,\mu$s, which is much longer than τ_{po}. The tail of the electron distribution is then collisionless. In earlier experiments where the electron temperature and pellet velocities were lower, τ_{ee}^E and τ_{po} were comparable and a collisional plasma response was dictated.

If a significant number of the electrons on a given flux surface interact directly with the pellet cloud during τ_{po}, their depletion will directly reduce the ablation rate. Let $\tilde{n}$ be the density of a group of electrons with one-sided particle flux $\tilde{J}$ in a flux tube of volume ΔV. The rate of depletion of these electrons through impact with the pellet cloud (assumed to be a perfect absorber) is given by

$$\frac{d\tilde{n}}{dt} \approx -\frac{\tilde{J}(2\pi r_o^2)}{\Delta V} \tag{45}$$

In a collisionless plasma, no source or loss terms associated with energy scattering are needed on the right side of Eq. (45); the characteristic flow velocity of a group of electrons is also constant. Let the initial density and particle flux far from the pellet be n and J; then,

$$\tilde{J}(t) \approx \tilde{n}(t) v_{\|} \tag{46}$$

Solving Eq. (45) for $\tilde{n}$ gives

$$\tilde{n}(t) = ne^{-t/\tau_d} \tag{47}$$

where

$$\tau_d^{-1} \equiv v_{\|} \frac{(2\pi r_o^2)}{\Delta V} \tag{48}$$

We may define an effective electron density, $\langle \tilde{n} \rangle$, by averaging over the interaction time, τ_{po}, giving

$$\frac{\langle \tilde{n} \rangle}{n} = \frac{\tau_d}{\tau_{po}} \left(1 - e^{-\tau_{po}/\tau_d}\right) \tag{49}$$

The reduction factor in Eq. (49) applies as well to the particle and energy fluxes to the pellet because of their linear dependence on density; thus, the reduced electron energy flux incident on the ionized cloud is related to the unperturbed electron energy flux by

$$Q_e^+ = Q_e \frac{\tau_d}{\tau_{po}} \left(1 - e^{-\tau_{po}/\tau_d}\right) \tag{50}$$

Applying the energy group structure of Section 4, we can evaluate the energy dependence of the depletion, τ_d/τ_{po}, for a set of nominal plasma conditions. The effective velocity at which electrons of energy group j intersect the ablation cloud can be approximated by

$$v_{\|} \approx \frac{\bar{v}_e}{4} \sqrt{\frac{E_{ej}}{E_e}} \approx \frac{\bar{v}_e}{4} \sqrt{\hat{E}_{ej}} \tag{51}$$

which reduces to $\bar{v}_e/4$ in a monoenergetic electron model.

The depletion on an irrational-q flux surface can be estimated by using an annular ring of plasma of thickness $2r_o$ at a (circular) plasma radius r in a torus of major radius R. Then $\Delta V = 8\pi^2 r r_o R$, so

$$\frac{\tau_{po}}{\tau_d} = \frac{\bar{v}_e}{v_p} \sqrt{\hat{E}_{ej}} \frac{r_o^2}{8\pi r R} \tag{52}$$

With $T_e = 2$ keV, $\hat{E}_{ej} = 2$, $r = 0.4$ m, $R = 2.5$ m, $r_o = 0.01$ m, and $v_p = 10^3$ m/s, then $\tau_{po}/\tau_d \approx 0.17$ and the averaged depletion is about 8%. Near the magnetic axis, depletion of electrons above thermal is almost complete.

In the vicinity of a rational flux surface, the volume is also more restricted (e.g., at the $q = 1$ surface ΔV is reduced by r_o/r in the preceding example). Higher-order rational surfaces should be seen, but finite shear and finite cloud size eventually diminish the effect.

6 SOLUTION TECHNIQUE

This method of solving the pellet ablation equations is conceptually the same as in earlier versions of the PELLET code [21]. The plasma is divided into a number of radial cells in which plasma properties are assumed uniform. The pellet path (straight-line trajectory) is mapped onto the plasma geometry [22], determining the chord length through each cell, the cell volumes, and the ambient plasma properties. From the chord lengths and pellet velocity, the time spent in each cell is determined. The pellet is then stepped along the trajectory, evolving the pellet radius by simultaneously satisfying the energy balance at the pellet surface, Eq. (1), and the hydrodynamics of the neutral cloud, Eq. (2). A number of details of the solution method, however, have been modified to accommodate multiple electron groups, fast ions from neutral beam injection and fast alphas, the ionized portion of the shield, and the collisionless approximation for self-limiting ablation.

After obtaining plasma geometry and pellet trajectory information, the group energies and densities of the fast beam ions and alphas are predetermined for each cell using Eqs. (32)–(43) or an equivalent time-dependent formalism [20]. The ambient electron density and temperature in each cell are determined, and dimensionless energy group parameters, Eqs. (29)–(31), are also set. When the pellet enters a new cell, the ambient electron density and temperature are adiabatically adjusted [21] if the pellet has passed through that cell in an earlier portion of the trajectory (e.g., after passing through the magnetic axis). The assumption here is that the electrons will have had time to reestablish a uniform Maxwellian distribution over the magnetic surface during the interval between intersections with that surface, regardless of whether the collisional or collisionless self-limiting approximation is used.

In the collisionless self-limiting model, the electron group densities and energy fluxes are then reduced by the depletion factor, Eqs. (49) and (50), assuming irrational flux surfaces everywhere. In the collisional self-limiting model, the ambient electron density and temperature in the cell are continuously adjusted [21]. The fast ion distributions are assumed to be unperturbed during the ablation process because their collisional and depletion timescales are typically much longer than the pellet lifetime.

The time evolution of the pellet radius is governed by a fourth-order Runge-Kutta routine that keeps the timestep small enough for pellet parameters (and plasma parameters in the collisional self-limiting approximation) to be changing weakly [21]. In each timestep, the line-integrated density in the neutral cloud is taken as the parameter of iteration until Eqs. (1) and (2) are simultaneously satisfied. A version of ZEROIN [23], modified for more rapid convergence by concentrating in the vicinity of a prior solution, determines the convergence. This numerical treatment differs from earlier versions of the pellet ablation model [4,21,5] that used the monoenergetic electron energy at the pellet surface as the iterating parameter.

The electrons are first passed through the ionized portion of the shield, reducing the energy and energy flux in each energy group according to Eqs. (23) and (25) respectively. This requires knowledge of the line-integrated density of the ionized shield, Eq. (20), which depends on the ablation rate, $\dot{N}$. The line-integrated density of the ionized shield is parameterized in terms of the line-integrated density of the neutral shield,

$$F_i \equiv \int_{r_o}^{\infty} n^+ dl \Big/ \int_{r_p}^{r_o} n^o dl \tag{53}$$

F_i is set by an initial condition upon first entering the plasma and subsequently reset from

the converged solution at the previous timestep. The electron energy and energy flux at the pellet surface are then determined from Eqs. (7)–(11) for each energy group, and fast hydrogenic ion and alpha energies are similarly determined by Eqs. (16) and (18). These are used to evaluate $\dot{r}_p$ from Eqs. (1) and (2). If the two solutions do not meet convergence criteria, the line-integrated density of the neutral shield is varied and the iteration proceeds.

Upon convergence, F_i is reset and a new timestep is taken until the pellet passes through the cell or becomes fully ablated. After the pellet completes its trip through the cell, the net deposition of mass in that cell is determined from the change in pellet radius.

The entire calculation (with multiple electron energy groups, fast neutral beam ions and alphas, and both ionized and neutral shields) typically takes less than 1 s of CPU time on a CRAY-1 computer and less than 5 s on a VAX 8600 (exclusive of plasma geometry and profile initialization and printed or graphic output). It is therefore convenient for routine data analysis and for incorporation in a transport code for modeling multiple pellet injection.

7 DISCUSSION

A more comprehensive treatment of electron distribution has long been viewed as an important step in improving the neutral shielding model for pellet ablation. As shown in Fig. 2, the stopping cross section for electrons falls off as E_e^{-1} above a few keV. A monoenergetic electron model that uses the Maxwellian-averaged electron energy of $3T_e/2$ then leads to low values of ablation rate in plasmas where temperatures exceed about 1 keV. In early ohmic heating experiments, this condition was not exceeded and the neutral shielding model was substantially confirmed [1,19]. In more recent experiments, larger, higher-velocity pellets have penetrated to regions of the plasma where electron temperatures approach 4 keV, and the monoenergetic electron model generally predicts somewhat greater penetration than observed [17].

We use TFTR machine and pellet parameters as a baseline for illustrating the various features and sensitivities of the revised pellet ablation model. The machine parameters for all cases are: major radius, 2.57 m; minor radius, 0.815 m; and plasma volume, 33.7 m^3. The density and electron temperature profiles and neutral beam parameters are from TRANSP analysis of shot No. 14695 at a time just before injection of a single pellet. This shot is of particular interest because its low density and the 2.5 MW of neutral beam injection initiated prior to pellet injection provide a reference point for evaluating fast ion effects. The density profile is relatively broad with $n_e(0) = 1.8 \times 10^{19}\,m^{-3}$, and the electron temperature profile is roughly triangular with $T_e(0) = 3.2$ keV. In cases where the electron temperature is varied, we simply scale the magnitude with the central temperature while maintaining the same shape. The nominal pellet parameters of shot No. 14695 are used unless specifically noted otherwise: $r_p = 1.53$ mm, $N = 8.9 \times 10^{20}$, and $v_p = 1.4$ km/s. In the experiment, the pellet penetrated about 60% of the distance to the axis and contained nearly twice the mass of the original plasma. In the following, the new features of the ablation model are added one at a time so their individual effects can be displayed.

Figure 3 shows the reduction in pellet penetration as the number of electron energy groups is increased. Fast beam ions are neglected, so the one-group results in Fig. 3a with adiabatic self-limiting ablation represent the standard model for most of our previous calculations. The increase to five groups greatly decreases the penetration, but above ten groups there is essentially no change in penetration. The predicted penetration for $T_e(0) = 3.2$ keV with multiple electron energy groups and the adiabatic self-limiting approximation is still above that observed experimentally. The adiabatic self-limiting effect is important in this case because of the high pellet-to-plasma mass ratio. Removal of this constraint leads to the results in Fig. 3b where penetration is below that observed experimentally. Plasma shielding, collisionless self-limiting ablation, and fast beam ion effects need to be considered before final conclusions can be drawn about agreement. In the remaining calculations, ten electron energy groups are used; each group carries 10% of the electron energy flux according to the prescription for selecting the groups given in Section 4.

To test the effect of an ionized shield, we arbitrarily fix the ratio of the line-integrated density in the ionized cloud relative to that in the neutral cloud [i.e., Eq. (53) is used rather than Eq. (20) to calculate the integrated line density in the ionized cloud]. In these cases, we do not include any self-limiting effects and we use ten electron energy groups. The ionized cloud leads to a reduced energy flux incident on the neutral cloud and a smaller line-integrated neutral density, reducing the ablation rate as shown in Fig. 4.

When the source strength at the pellet surface and the effective ionization radius are used to determine the line density in the plasma shield, Eq. (20), the results of Fig. 5 are

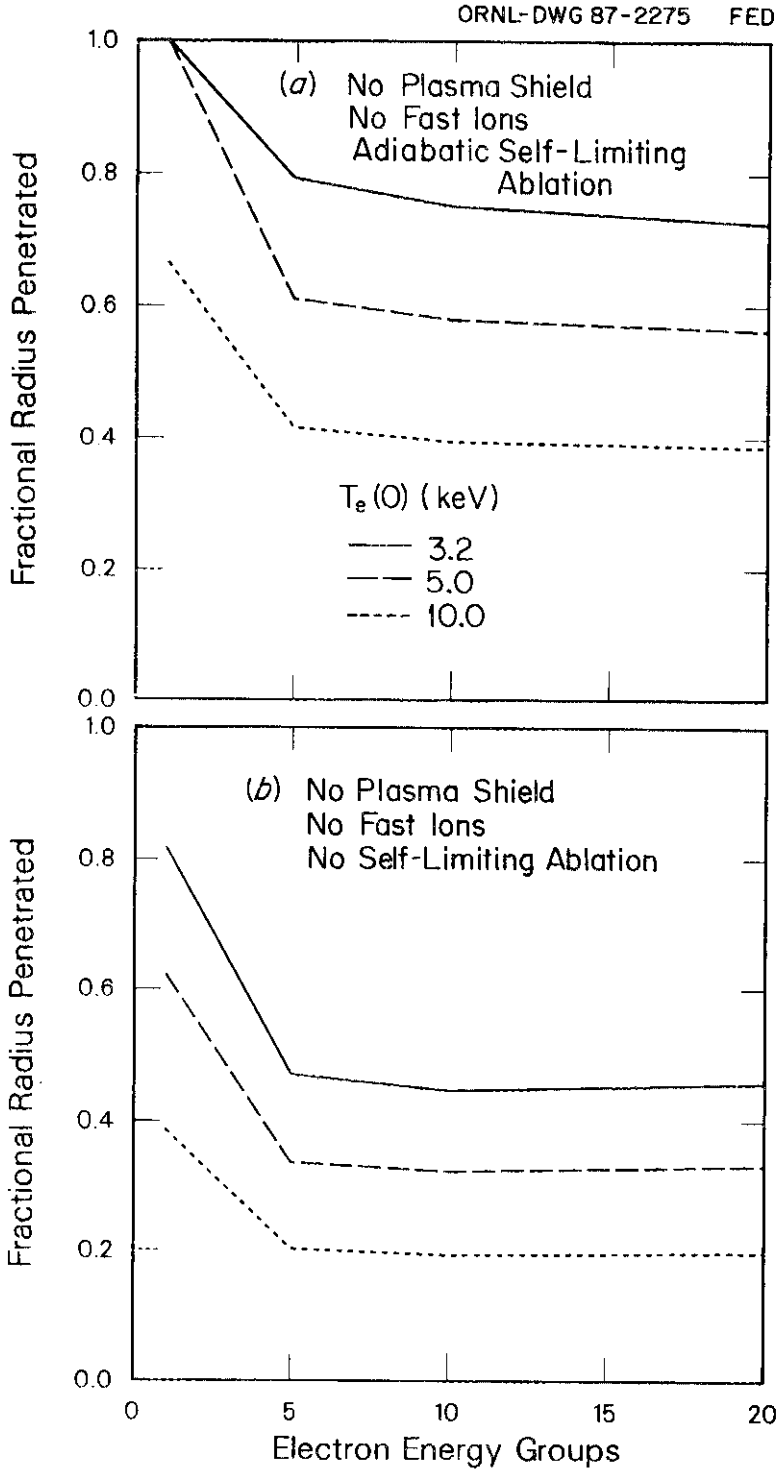

Figure 3: Increasing the number of electron energy groups in a multigroup treatment of the electron distribution function decreases the calculated pellet penetration depth. At ten groups the effect is nearly saturated. The one-group result is the monoenergetic neutral shielding electron model with adiabatic self-limiting ablation.

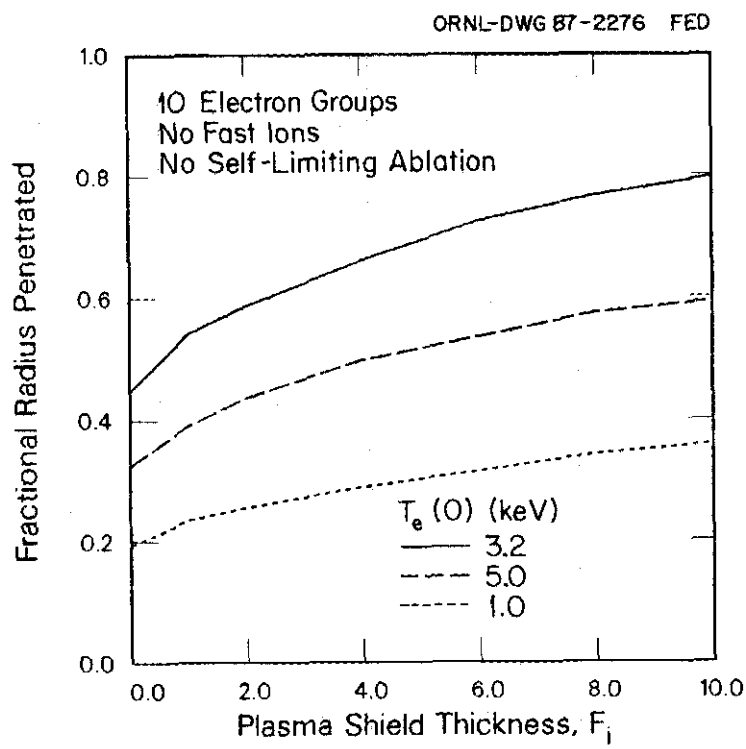

Figure 4: Addition of an ionized shield extending along the magnetic field reduces ablation. A line-integrated density in the ionized shield equal to the line-integrated density in the neutral shield ($F_i = 1$) improves penetration by about 10%. Further increases in the ionized shield lead to even greater pellet penetration.

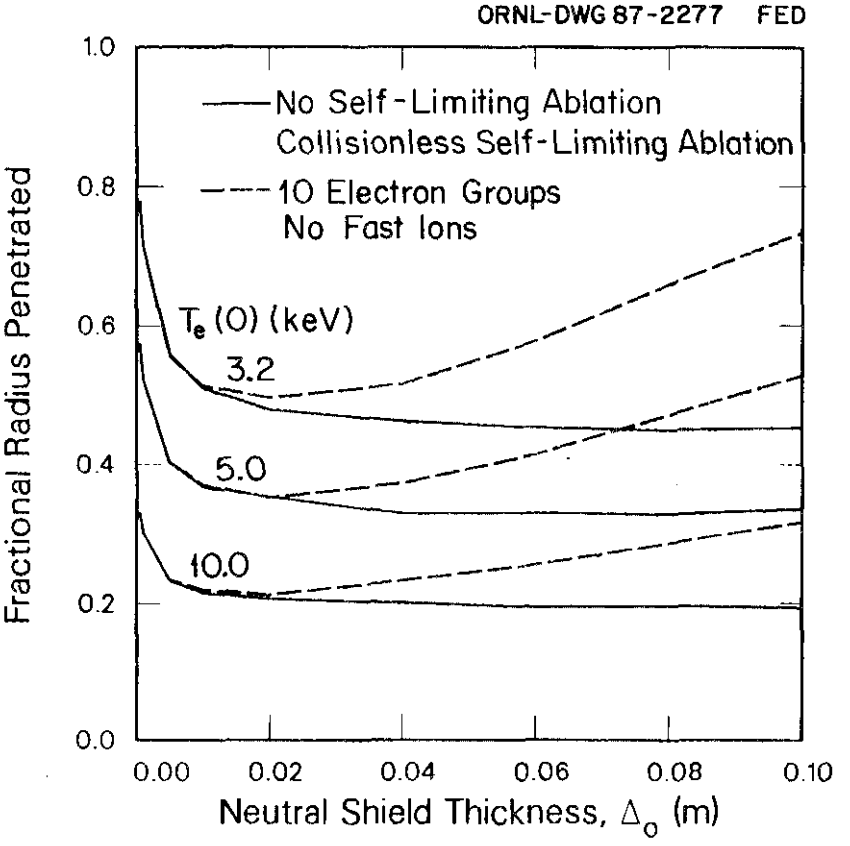

Figure 5: Penetration is enhanced as the thickness of the neutral gas layer is reduced below about 2 cm because the ionized ablatant is constrained to a smaller-diameter tube. In the outer half of the plasma, collisionless self-limiting ablation (dashed curves) is important only if the ionization radius is very large.

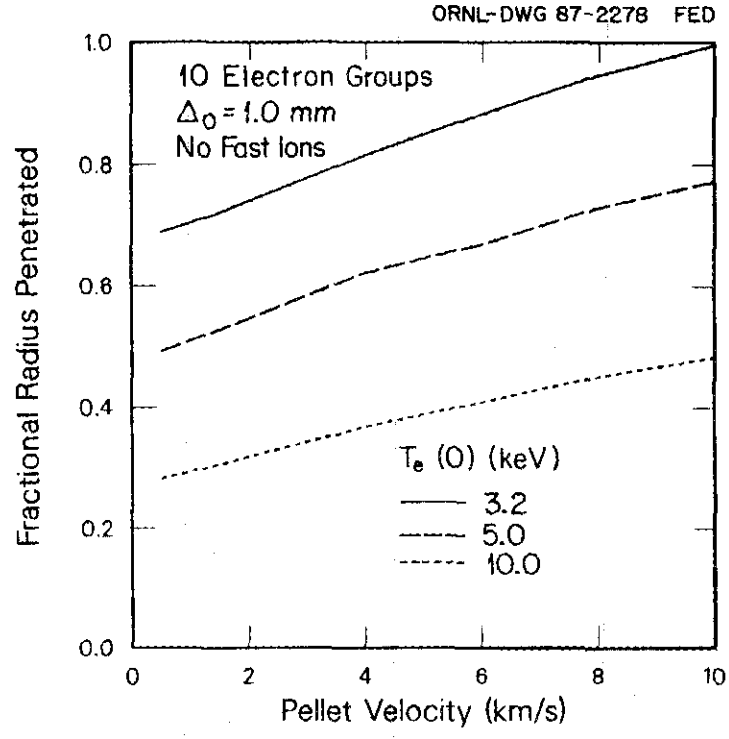

Figure 6: Modest gains in pellet penetration are realized with increasing velocity.

obtained. As the neutral shield thickness, Δ_o, is decreased below $\approx$1 cm, plasma shielding becomes important because the ablatant is highly concentrated in a narrow tube. The JET pellet injection results [16,17] are best modeled with $\Delta_o = 1$ mm, which corresponds to significant plasma shielding. For larger effective ionization radii, the plasma shield is more diffuse and the non-self-limiting results (solid curves) approach those of Fig. 4 in the limit $F_i = 0$.

The dashed curves of Fig. 5 show the effect of including collisionless self-limiting ablation as expressed by Eq. (50). As the pellet cloud size is increased, a larger fraction of the electrons interacts with the ablatant, and significant depletion of the energetic electrons leads to enhanced pellet penetration. For ionization radii above a few centimeters, the implicit assumption that all electrons intercepted by the cloud lose all their energy to the ablatant is not valid because the ablatant is too diffuse to stop the electrons. At $\Delta_o = 1$ mm, the effect of collisionless self-limiting ablation is negligible in these cases because the pellet penetrates only the outer region of the plasma where the intercepted plasma volume is large (irrational flux surfaces are assumed). Self-limiting ablation does become important near the magnetic axis (in cases not presented here) and should also be considerable at low-order rational surfaces although we have not attempted to model this effect.

The gain in penetration with increasing pellet velocity is shown in Fig. 6 for $T_e(0) = 3.2$, 5.0, and 10.0 keV, using $\Delta_o = 1$ mm and ignoring fast ion contributions. Although higher pellet velocity provides only a modest increase in penetration, it could be important for increased control over the density profile and for avoiding high deposition and cooling at rational surfaces where MHD activity could be enhanced.

Even though fast ions may represent only a small contribution to the one-sided energy

flux in the plasma, they may lead to enhanced ablation at the pellet surface if the shield set up by the electrons is insufficient to stop them. This is illustrated in Fig. 7 where the solutions for $\dot{r}_p$ from Eqs. (1) and (2) are plotted against a dimensionless neutral cloud line density,

$$\hat{n}^o \equiv \frac{\int_{r_p}^{r_o} n^o dl}{2 n_s^m r_{po}} \tag{54}$$

where r_{po} is the initial pellet radius and n_s^m is the molecular density of the solid pellet. This analysis is similar to that presented by Milora and Foster [4] except that the solution is expressed in terms of $\hat{n}^o$ (instead of the electron energy at the pellet surface) and that fast ions are included.

For simplicity, we consider only neutral shielding effects and a background plasma of $T_e = 0.2\,\mathrm{keV}$ and $n_e = 5.0 \times 10^{19}\,\mathrm{m}^{-3}$. The fast deuterium ions have a slowing-down distribution and a source at $E_{io} = 120\,\mathrm{keV}$ with an intensity of $0.45\ \mathrm{MW/m^3}$. The solution for $\dot{r}_p$ from Eq. (2) is proportional to $\hat{n}^o$ for very low $\hat{n}^o$ and $(\hat{n}^o)^{2/3}$ for high values. The solution of Eq. (2) is insensitive to the addition of fast ions in this example because the fast ions constitute a small contribution to the total energy flux. With a very low line-integrated neutral shield density, all the energy flux reaches the pellet surface, $Q^p = Q^+$; the solution for $\dot{r}_p$ from Eq. (1) is proportional to Q^+ and independent of the line-integrated neutral cloud density. By comparing the solutions with and without fast ions in this limit, it can be seen that the one-sided fast ion energy flux in the plasma is very small, $Q_i^+ \ll Q_e^+$. As $\hat{n}^o$ is increased, the electrons are the first to be stopped; the critical line density is $\hat{n}_{ec}^o \approx 1.0 \times 10^{-4}$ as seen from the solution without fast ion effects. The critical line density for 120-keV deuterium ions is much larger, $\hat{n}_{ic}^o \approx 2.0 \times 10^{-3}$, and increases the self-consistent solution [the intersection of the solutions to Eqs. (1) and (2)] from $\dot{r}_p = 0.5\,\mathrm{m/s}$ to $2.0\,\mathrm{m/s}$.

There are two criteria for determining whether fast ions are important, and these can be expressed in relatively concise form from the neutral shielding solution. The first is that the neutral shield line density for stopping fast ions must be greater than that for stopping electrons. This critical value for hydrogenic ions can be obtained from Eq. (16) by setting $E_i^p = 0$ for the most energetic ions,

$$\begin{aligned} \int n^o dl \Big|_{ic} &= a_{i2} E_{io} + 2 a_{i1} \sqrt{A_i E_{io}} \\ &\approx 2 a_{i1} \sqrt{A_i E_{io}} \end{aligned} \tag{55}$$

where the approximation is valid for all relevant neutral beam injection energies. Similarly, the critical value for electrons is approximated by setting $E_e^p = 0$ in Eq. (6),

$$\begin{aligned} \int n^o dl \Big|_{ec} &= a_{e1} E_e^o + \frac{a_{e2}}{2} E_e^{o2} \\ &\approx \frac{a_{e2}}{2} E_e^{o2} \end{aligned} \tag{56}$$

where the approximation is valid for $E_e^o \geq 2\,\mathrm{keV}$. E_e^o is taken as the energy of electrons in the tail of the distribution; the average energy of tail electrons representing 10% of the energy flux is $E_e^o \approx 6.4 T_e$. The condition for fast ions to be important then leads to a constraint on E_{io} in terms of T_e:

$$A_i E_{io} \geq 175 T_e^4 \tag{57}$$

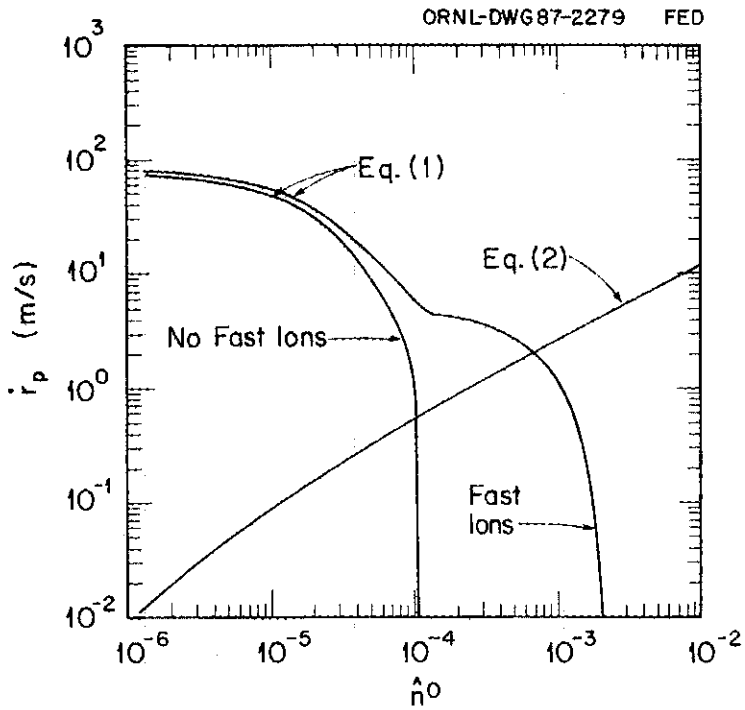

Figure 7: Pellet surface erosion rates from the energy source at the pellet surface given by Eq. (1) and the neutral shield solution given by Eq. (2) as a function of the dimensionless neutral shield density show how fast ions with a low energy flux can increase pellet ablation. The self-consistent solution is given by the intersection of the two sets of curves in each case.

It can be seen that, with present beam injection energies, fast ions should be important only in the outer plasma region where $T_e \leq 1\,\mathrm{keV}$. This conclusion concurs with that of Nakamura et al. [7].

The second condition is that the fast ion energy flux to the pellet surface, Q_i^+, must be greater than the electron energy flux to the pellet surface, Q_e^+, in the absence of fast ions. This can be the case even if the one-sided fast ion energy flux in the plasma is much lower than that of the electrons. Typically, the neutral shield reduces the electron energy flux by more than two orders of magnitude, as can be seen in Fig. 7; let this electron shielding factor be f_e. Since we are looking for a regime in which the fast ions are unshielded [i.e., Eq. (57) is satisfied and $f_i = 1$], we can use the condition

$$Q_i^p \approx Q_i^+ \geq Q_e^p = f_e Q_e^+ \tag{58}$$

to determine when fast beam ions become important. From the expressions for the energy fluxes in Section 4, we obtain

$$\frac{Q_i^+}{Q_e^+} = 2.51 \times 10^{31} \frac{H(r) P_b}{V_p n_e^2} (A_i E_{io})^{1/2} \geq f_e \tag{59}$$

For the example in Fig. 7, $Q_i^+/Q_e^+ = 0.07$, which is an order of magnitude greater than the electron shielding factor of $f_e = 0.007$. The observation that fast ion effects are most prominent at low T_e, Eq. (57), and low n_e, Eq. (59), is in accord with the conclusions of Nakamura et al. [7].

The conditions given by Eqs. (57) and (59) assume only a neutral shield (or that the ions and electrons see the same shield). If a relatively large portion of the electron shielding comes from the ionized shield while fast ions see only the neutral shield, the threshold for fast ion effects is reduced. In the outer plasma regions where fast ion effects may be expected, however, the neutral shield is dominant and the above conditions should yield a good estimate of the threshold for fast ion effects. If Eq. (57) is not satisfied, the fast ion energy flux must be comparable to the electron energy flux; the influence of the fast ions is felt through the energy balance in the neutral shield, Eq. (2), and is a much weaker effect.

Figure 8 shows the effect of increasing beam power on pellet penetration for the TFTR case being examined. The reference model consists of ten electron groups, a plasma shield determined by a neutral shield thickness of 1 mm, and collisionless self-limiting ablation of the electrons. The plasma electron temperature and density profiles are kept constant as the beam power is increased. Deuterium beam injection at $E_{io} = 79\,\mathrm{keV}$ is used. The power splits for the full, half, and one-third energy components are 0.45 : 0.30 : 0.25 with the $H(r)$ profiles determined by the plasma density profile and TFTR beam geometry for shot No. 14695. Because the enhanced ablation from fast ions is concentrated in the edge region where charge-exchange losses can play an important role in determining the fast ion population, we also show the effect of varying the flux-surface-averaged neutral density at the plasma edge. With $n_o(a) \approx 3.0 \times 10^{14}\,\mathrm{m}^{-3}$ as expected from transport analysis of this shot, the charge-exchange losses are negligible and the calculated penetration with 2.5 MW is in excellent agreement with the observed penetration. Figure 9 shows a comparison of the time-dependent ablation rate curves with and without the 2.5 MW of neutral beam heating. The fast ion enhancement in the outer region is characteristically observed on the H_α signals. $Q_i^+/Q_e^+ \simeq 0.05$–0.4 over the region of enhanced ablation because of the very low initial plasma density.

Threshold criteria for enhanced ablation by fast alphas similar to those derived above for fast beam ions can be used to show that alpha particles undergoing classical, local

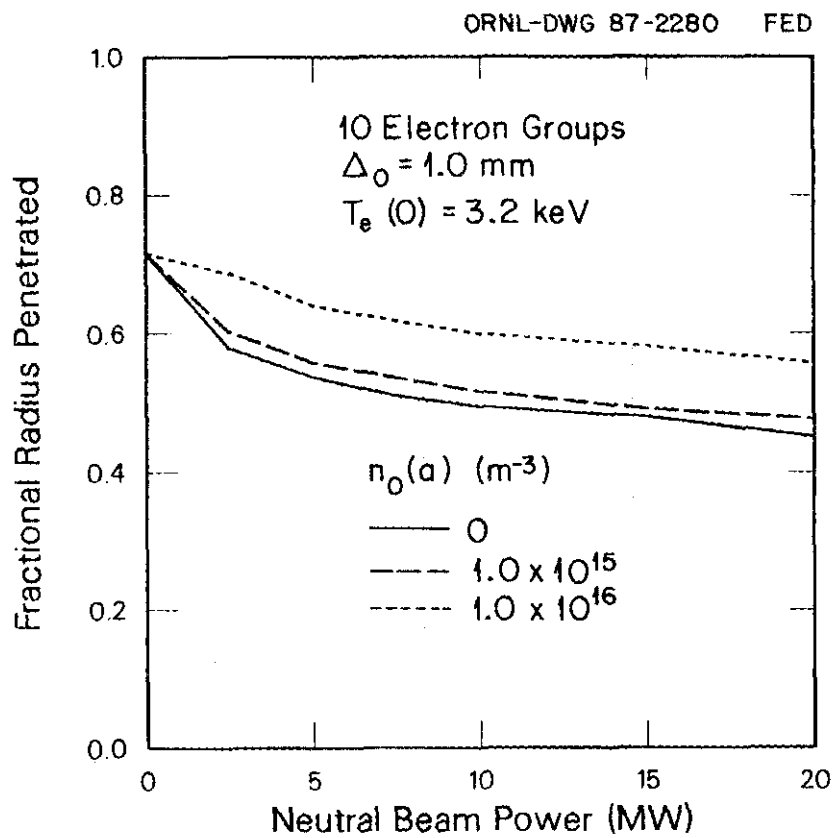

Figure 8: Enhanced ablation from fast neutral beam injected ions in TFTR is expected at a very low power threshold and is sensitive to charge-exchange losses because fast ion effects are concentrated in the plasma periphery.

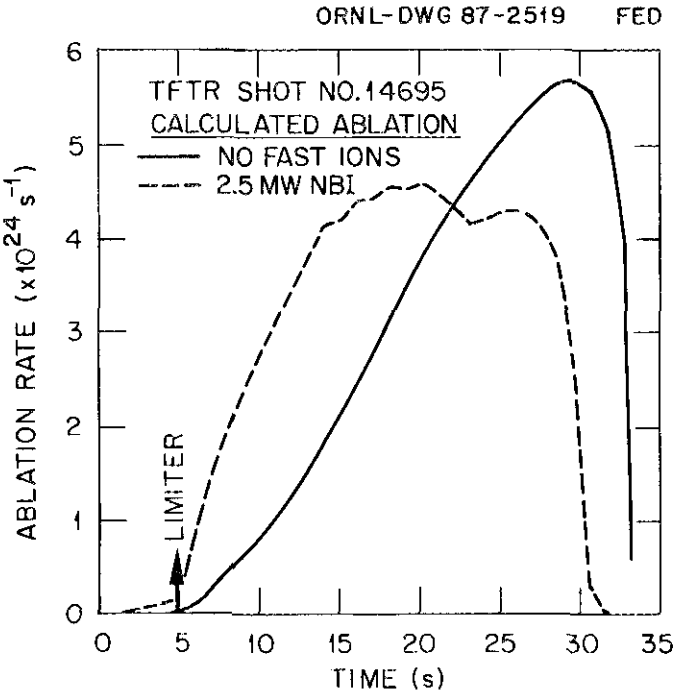

Figure 9: Fast ions from neutral beam injection can lead to enhanced ablation in the outer regions of TFTR plasmas.

thermalization should not contribute to pellet ablation. The critical line-integrated density in the neutral shield for stopping 3.5-MeV alphas is obtained from Eq. (18) with $E_\alpha^p = 0$:

$$\int n^o dl\Big|_{\alpha c} = \frac{E_\alpha^{o(1-a_{\alpha 2})}}{a_{\alpha 1}(1-a_{\alpha 2})}$$
$$= 3.6 \times 10^{24}\,\mathrm{m}^{-2} \tag{60}$$

Requiring this to be greater than the critical line-integrated density for stopping high-energy tail electrons leads to an upper limit on the local electron temperature for alphas to be important,

$$T_e \leq 4.7\,\mathrm{keV} \tag{61}$$

By using $n_e^2\langle\sigma v\rangle_{DT}/4$ as the local source strength for fast alphas, it can be shown that the ratio of the one-sided energy fluxes in the plasma is

$$\frac{Q_\alpha^+}{Q_e^+} \propto \langle\sigma v\rangle_{\mathrm{DT}} \tag{62}$$

for a classical, local slowing-down distribution. Q_α^+ is only 0.22% of Q_e^+ at $T_e = 4.7\,\mathrm{keV}$. Therefore, alphas may contribute to the ablation process only if their population exceeds that expected from thermal reactions (e.g., when beam-beam or beam-plasma interactions dominate or when large orbits or direct losses carry energetic alphas to the outer regions of the plasma).

8 SUMMARY

We have extended the original neutral shielding model by including a more complete treatment of electron and fast ion distributions and including a plasma shield extending along the magnetic field lines. The only "free" parameter in the model is the effective ionization radius expressed in terms of the thickness of the neutral shield, Δ_o. The value of Δ_o required to match experimental results is quite small, but it appears to be supported by experimental observations.

One difference between our model for the plasma shield and that of Kaufmann et al. is in the treatment of energy transport through the ionized shield. We treat the energetic electrons from the plasma as a distribution of test particles slowing down in a cold electron target, while Kaufmann et al. use a single fluid for the electrons and consider energy flow to be dominated by conduction. The single-fluid treatment of the electrons leads to a low value for energy flow in the outer portions of the shield and thus a greatly reduced ablation rate. Our multiple energy group model is more appropriate for the outer portions of the shield, but it is not justifiable if the energy of plasma electrons is reduced to that of the ablatant electrons. A full and proper treatment of the kinetics of the combined neutral and plasma shield remains to be done. Nevertheless, the multigroup approximation has been successful in matching experimental results and provides a useful tool for predicting penetration distances under a wide range of plasma conditions.

Many individual shots from ISX, PDX, Alcator-C, PLT, D-III, and TFTR have been analyzed with the PELLET code during its development and are currently undergoing more extensive analysis for a subsequent report. The most systematic single-machine analysis to date has been performed on JET; results of the analysis will be reported elsewhere [17].

REFERENCES

[1] S. L. Milora, *J. Fusion Energy* **1**, 15 (1981).

[2] C. T. Chang, L. W. Jorgensen, P. Nielsen, and L. L. Lengyel, *Nucl. Fusion* **20**, 859 (1980).

[3] P. B. Parks, R. J. Turnbull, and C. A. Foster, *Nucl. Fusion* **17**, 539 (1977).

[4] S. L. Milora and C. A. Foster, *IEEE Trans. Plasma Sci.* **PS-6**, 578 (1978).

[5] S. L. Milora, ORNL/TM-8616, Oak Ridge National Lab. (1983).

[6] S. L. Milora, C. A. Foster, C. E. Thomas, C. E. Bush, J. B. Wilgen, E. A. Lazarus, J. L. Dunlap, P. H. Edmonds, W. A. Houlberg, H. C. Howe, D. P. Hutchinson, T. C. Jernigan, M. Murakami, G. H. Neilson, J. A. Rome, and M. J. Saltmarsh, *Nucl. Fusion* **20**, 1481 (1980).

[7] Y. Nakamura, H. Nishihara, and M. Wakatani, *Nucl. Fusion* **26**, 907 (1986).

[8] M. Kaufmann, K. Lackner, L. L. Lengyel, and W. Schneider, *Nucl. Fusion* **26**, 171 (1986).

[9] P. C. Souers, *Hydrogen Properties for Fusion Energy* (University of California Press, 1986).

[10] M. G. Heaps and A. E. S. Green, *J. Appl. Phys.* **46**, 4718 (1975).

[11] C. F. Barnett, J. A. Ray, E. Ricci, M. I. Wilker, E. W. McDaniel, E. W. Thomas, and H. B. Gilbody, ORNL/TM-5206, Oak Ridge National Lab. Rep. (February 1977).

[12] P. B. Parks, *Nucl. Fusion* **20**, 311 (1980).

[13] C. E. Thomas, ORNL/TM-7486, Oak Ridge National Lab. (1981).

[14] D. H. McNeill, G. J. Greene, and D. D. Schuresko, *Phys. Rev. Lett.* **55**, 1398 (1985).

[15] TFR Group, *Europhys. Lett.* **2**, 267 (1986).

[16] A. Gondhalekar, A. Cheetham, M. Bures, D. Campbell, S. A. Cohen, G. Cordey, S. Corti, A. Edwards, J. Ehrenberg, R. Gill, R. Granetz, F. Hendriks, W. Houlberg, H. Jackel, T. Jones, M. Keilhacker, G. Magyar, P. Mantica, V. Mertens, P. D. Morgan, P. Nielsen, J. O'Rourke, G. Sadler, F. C. Schuller, M. Stamp, A. Tanga, P. R. Thomas, M. L. Watkins, and A. Weller, Pellet Fueling of JET Plasmas During Ohmic, ICRF and NBI Heating, in Plasma Physics and Controlled Nuclear Fusion Research (Proc. 11th Int. Conf., Kyoto, 1986), paper I-I-6, to be published.

[17] M. L. Watkins, W. A. Houlberg, A. D. Cheetham, A. Gondhalekar, R. Granetz, F. Hendriks, J. O'Rourke, and P. M. Stubberfield, A Model for Pellet Ablation in JET, in Controlled Fusion and Plasma Physics (Proc. 14th Europ. Conf., Madrid, 1987), to be published.

[18] W. W. Heidbrink, S. L. Milora, G. L. Schmidt, W. Schneider, and A. Ramsey, *Nucl. Fusion* **27**, 3 (1987).

[19] M. Greenwald, J. Parker, J. Bensen, C. L. Fiore, M. Foord, R. Gandy, R. S. Granetz, D. Gwinn, B. Lipshhultz, B. Labombard, B. Lloyd, E. S. Marmar, S. McCool, S. L. Milora, D. S. Pappas, R. R. Parker, R. Petrasso, P. A. Politzer, M. Porkobab, P. Pribyl, J. E. Rice, D. Schuresko, J. J. Schuss, J. L. Terry, S. Texter, R. Watterson, and S. M. Wolfe, in *Controlled Fusion and Plasma Physics (Proc. 11th Europ. Conf., Aachen, 1983)*, p. 7 (European Physical Society, 1983).

[20] S. E. Attenberger and W. A. Houlberg, *Nucl. Technol./Fusion* 4, 129 (1983).

[21] W. A. Houlberg, M. A. Iskra, H. C. Howe, and S. E. Attenberger, ORNL/TM-6549, Oak Ridge National Lab. (1979).

[22] S. E. Attenberger, W. A. Houlberg, and S. P. Hirshman, Some Practical Considerations Involving Spectral Representations of 3-D Plasma Equilibria, to be published in J. Comput. Phys.

[23] G. E. Forsythe, M. A. Malcolm, and C. B. Moler, *Computer Methods for Mathematical Computations*, p. 161, Prentice-Hall, New Jersey, 1977.

ORNL/TM-10556
Dist. Category UC-20 g

1. L. A. Berry
2. B. A. Carreras
3. S. K. Combs
4. R. A. Dory
5. C. A. Foster
6. R. H. Fowler
7. M. J. Gouge
8. H. H. Haselton
9. J. T. Hogan
10. H. C. Howe
11. T. C. Jernigan
12. Y-K. M. Peng
13. D. D. Schuresko
14. J. Sheffield
15. J. S. Tolliver
16. G. E. Whitesides
17. J. B. Wilgen
18. N. A. Uckan
19. Laboratory Records Department
20. Laboratory Records, ORNL-RC
21. Document Reference Section
22. Central Research Library
23. Fusion Energy Division Library
24-25. Fusion Energy Division Publications Office
26. ORNL Patent Office

EXTERNAL DISTRIBUTION

27. Office of the Assistant Manager for Energy Research and Development, U.S. Department of Energy, Oak Ridge Operations Office, P. O. Box E, Oak Ridge, TN 37831
28. J. D. Callen, Department of Nuclear Engineering, University of Wisconsin, Madison, WI 53706-1687
29. J. F. Clarke, Director Office of Fusion Energy, Office of Energy Research, ER-50 Germantown, U.S. Department of Energy, Washington, DC 20545
30. R. W. Conn, Department of Chemical, Nuclear, and Thermal Engineering, University of California, Los Angeles, CA 90024
31. S. O. Dean, Fusion Power Associates, 2 Professional Drive, Suite 248, Gaithersburg, MD 20879
32. H. K. Forsen, Bechtel Group, Inc., Research Engineering, P. O. Box 3965, San Francisco, CA 94105
33. J. R. Gilleland, GA Technologies, Inc., Fusion and Advanced Technology, P.O. Box 81608, San Diego, CA 92138
34. R. W. Gould, Department of Applied Physics, California Institute of Technology, Pasadena, CA 91125
35. R. A. Gross, Plasma Research Laboratory, Columbia University, New York, NY 10027
36. D. M. Meade, Princeton Plasma Physics Laboratory, P.O. Box 451, Princeton, NJ 08544
37. M. Roberts, International Programs, Office of Fusion Energy, Office of Energy Research, ER-52 Germantown, U.S. Department of Energy, Washington, DC 20545
38. W. M. Stacey, School of Nuclear Engineering and Health Physics, Georgia Institute of Technology, Atlanta, GA 30332
39. D. Steiner, Nuclear Engineering Department, NES Building, Tibbetts Avenue, Rensselaer Polytechnic Institute, Troy, NY 12181

40. R. Varma, Physical Research Laboratory, Navrangpura, Ahmedabad 380009, India
41. Bibliothek, Max-Planck Institut fur Plasmaphysik, D-8046 Garching, Federal Republic of Germany,
42. Bibliothek, Institut fur Plasmaphysik, KFA, Postfach 1913, D-5170 Julich, Federal Republic of Germany,
43. Bibliotheque, Centre de Recherches en Physique des Plasmas, 21 Avenue des Bains, 1007 Lausanne, Switzerland
44. F. Prevot, CEN/Cadarache, Departement de Recherches sur la Fusion Controlee, F-13108 Saint-Paul-lez-Durance Cedex, France
45. R. Aymar, CEA/Cadarache, Departement de Recherches sur la Fusion Controlee, F-13108 Saint-Paul-lez-Durance Cedex, France
46. J. Tachon, CEA/Cadarache, Department de Recherches sur la Fusion Controlee, F-13108 Saint-Paul-lez-Durance Cedex, France
47. Documentation S.I.G.N., Departement de la Physique du Plasma et de la Fusion Controlee, Centre d'Etudes Nucleaires, B.P. 85, Centre du Tri, F-38031 Grenoble, France
48. M. G. Claudet, Departement de la Physique du Plasma et de la Fusion Controlee, Centre d'Etudes Nucleaires, B.P. 85, Centre du Tri, F-38031 Grenoble, France
49. J. Lafferarderie, Departement de la Physique du Plasma et de la Fusion Controlee, Centre d'Etudes Nucleaires, B.P. 85, Centre du Tri, F-38031 Grenoble, France
50. Library, Culham Laboratory, UKAEA, Abingdon, Oxfordshire, OX14 3DB, England
51. Library, FOM-Instituut voor Plasma-Fysica, Rijnhuizen, Edisonbaan 14, 3439 MN Nieuwegein, The Netherlands
52. Library, Institute of Plasma Physics, Nagoya University, Nagoya 464, Japan
53. Library, International Centre for Theoretical Physics, P.O. Box 586, I-34100 Trieste, Italy
54. Library, Laboratorio Gas Ionizatti, CP 56, I-00044 Frascati, Rome, Italy
55. Library, Plasma Physics Laboratory, Kyoto University, Gokasho, Uji, Kyoto, Japan
56. Y. Nakamura, Plasma Physics Laboratory, Kyoto University, Gokasho, Uji, Kyoto, Japan
57. M. Wakatani, Plasma Physics Laboratory, Kyoto University, Gokasho, Uji, Kyoto, Japan
58. S. Sudo, Plasma Physics Laboratory, Kyoto University, Gokasho, Uji, Kyoto, Japan
59. G. A. Emmert, University of Wisconsin - Madison, Sterling Hall, Room 429, 1150 University Avenue, Madison, WI 53706
60. W. L. Rowan, The University of Texas at Austin, Fusion Research Center, RLM 11.222, Austin, TX 78712
61. Plasma Research Laboratory, Australian National University, P.O. Box 4, Canberra, A.C.T. 2000, Australia
62. Thermonuclear Library, Japan Atomic Energy Research Institute, Tokai Establishment, Tokai-mura, Naka-gun, Ibaraki-ken, Japan

63. G. A. Eliseev, I. V. Kurchatov Institute of Atomic Energy, P.O. Box 3402, 123182 Moscow, U.S.S.R.

64. V. A. Glukhikh, Scientific-Research Institute of Electro-Physical Apparatus, 188631 Leningrad, U.S.S.R.

65. I. Shpigel, Institute of General Physics, U.S.S.R. Academy of Sciences, Ulitsa Ulitsa Vavilova 38, Moscow, U.S.S.R.

66. D. D. Ryutov, Institute of Nuclear Physics, Siberian Branch of the Academy of Sciences of the U.S.S.R., Sovetskaya St. 5, 630090 Novosibirsk, U.S.S.R.

67. V. T. Tolok, Kharkov Physical-Technical Institute, Academical St. 1, 310108 Kharkov, U.S.S.R.

68. Library, Academia Sinica, P.O. Box 3908, Beijing, China (PRC)

69. D. Crandall, Experimental Plasma Research Branch, Division of Development and Technology, Office of Fusion Energy, Office of Energy Research, ER-542 Germantown, U.S. Department of Energy, Washington, DC 20545

70. N. A. Davies, Office of the Associate Director, Office of Fusion Energy, Office of Energy Research, ER-51 Germantown, U.S. Department of Energy, Washington, DC 20545

71. D. B. Nelson, Director, Division of Applied Plasma Physics, Office of Fusion Energy, Office of Energy Research, ER-54 Germantown, U.S. Department of Energy, Washington, DC 20545

72. E. Oktay, Division of Confinement Systems, Office of Fusion Energy, Office of Energy Research, ER-55 Germantown, U.S. Department of Energy, Washington, DC 20545

73. W. Sadowski, Fusion Theory and Computer Services Branch, Division of Applied Plasma Physics, Office of Fusion Energy, Office of Energy Research, ER-541 Germantown, U.S. Department of Energy, Washington, DC 20545

74. P. M. Stone, Fusion Systems Design Branch, Division of Development and Technology, Office of Fusion Energy, Office of Energy Research, ER-532 Germantown, U.S. Department of Energy, Washington, DC 20545

75. J. M. Turner, International Programs, Office of Fusion Energy, Office of Energy Research, ER-52 Germantown, U.S. Department of Energy, Washington, DC 20545

76. R. E. Mickens, Atlanta University, Department of Physics, Atlanta, GA 30314

77. M. N. Rosenbluth, RLM 11.218, Institute for Fusion Studies, University of Texas, Austin, TX 78712

78. Duk-In Choi, Department of Physics, Korea Advanced Institute of Science and Technology, P.O. Box 150, Chong Ryang-Ri, Seoul, Korea

79. Theory Department Read File, c/o D. W. Ross, University of Texas, Institute for Fusion Studies, Austin, TX 78712

80. Theory Department Read File, c/o R. C. Davidson, Director, Plasma Fusion Center, NW 16-202, Massachusetts Institute of Technology, Cambridge, MA 02139

81. R. R. Parker, Plasma Fusion Center, NW 16-288, Massachusetts Institute of Technology, Cambrige, MA 02139

82. M. Greenwald, Plasma Fusion Center, NW 16-274, Massachusetts Institute of Technology, Cambridge, MA 02139

83. Theory Department Read File, c/o R. White, Princeton Plasma Physics Laboratory, P.O. Box 451, Princeton, NJ 08544

84. Library of Physics Department, University of Ioannina, Ioannina, Greece

85. Theory Department Read File, c/o L. Kovrizhnykh, Lebedev Institute of Physics, Academy of Sciences, 53 Leninsky Prospect, 117924 Moscow, U.S.S.R.

86. Theory Department Read File, c/o B. B. Kadomtsev, I. V. Kurchatov Institute of Atomic Energy, P.O. Box 3402, 123182 Moscow, U.S.S.R.

87. Theory Department Read File, c/o T. Kamimura, Institute of Plasma Physics, Nagoya University, Nagoya 464, Japan

88. Theory Department Read File, c/o C. Mercier, Departemente de Recherches sur la Fusion Controlee, B.P. No. 6, F-92260 Fontenay-aux-Roses (Seine), France

89. Theory Department Read File, c/o T. E. Stringer, JET Joint Undertaking, Culham Laboratory, Abingdon Oxfordshire, OX14 3DB, England

90. Theory Department Read File, c/o R. Briscoe, Culham Laboratory, Abingdon, Oxfordshire OX14 3DB, England

91. Theory Department Read File, c/o D. Biskamp, Max-Planck-Institut fur Plasmaphysik, D-8046 Garching, Federal Republic of Germany

92. L. L. Lengyel, Max-Planck-Institut fur Plasmaphysik, D-8046 Garching, Federal Republic of Germany

93. M. Kaufmann, Max-Planck-Institut fur Plasmaphysik, D-8046 Garching, Federal Republic of Germany

94. K. Büchl, Max-Planck-Institut fur Plasmaphysik, D-8046 Garching, Federal Republic of Germany

95. B. G. Logan, Lawrence Livermore National Laboratory, Magnetic Fusion Energy Program, P.O. Box 5511 L-644, Livermore, CA 94550

96. L. J. Perkins, Lawrence Livermore National Laboratory, Magnetic Fusion Energy Program, P.O. Box 5511, Livermore, CA 94550

97. Theory Department Read File, c/o T. Takeda, Japan Atomic Energy Research Institute, Tokai Establishment, Tokai-mura, Naka-gun, Ibaraki-ken, Japan

98. S. Sengoku, Japan Atomic Energy Research Institute, Tokai Establishment, Tokai-mura, Naka-gun, Ibaraki-ken, Japan

99. M. Nagarni, Japan Atomic Energy Research Institute, Tokai Establishment, Tokai-mura, Naka-gun, Ibaraki-ken, Japan

100. S. Kasai, Japan Atomic Energy Research Institute, Tokai Establishment, Tokai-mura, Naka-gun, Ibaraki-ken, Japan

101. Theory Department Read File, c/o J. Greene, GA Technologies, Inc., P.O. Box 81608, San Diego, CA 92138

102. Theory Department Read File, c/o L. D. Pearlstein, L-630, Lawrence Livermore National Laboratory, P.O. Box 5511, Livermore, CA 94550

103. Theory Department Read File, c/o R. Gerwin, CTR Division, Los Alamos National Laboratory, P.O. Box 1663, Los Alamos, NM 87545

104. G. J. Greene, Princeton Plasma Physics Laboratory, P.O. Box 451, Princeton, NJ 08544

105. D. E. Post, Princeton Plasma Physics Laboratory, P.O. Box 451, Princeton, NJ 08544

106. G. L. Schmidt, Princeton Plasma Physics Laboratory, P.O. Box 451, Princeton, NJ 08544

107. D. K. Owens, Princeton Plasma Physics Laboratory, P.O. Box 451, Princeton, NJ 08544

108. W. W. Heidbrink, Princeton Plasma Physics Laboratory, P.O. Box 451, Princeton, NJ 08544

109. R. G. Bateman, Princeton Plasma Physics Laboratory, P.O. Box 451, Princeton, NJ 08544

110. C. K. Phillips, Princeton Plasma Physics Laboratory, P.O. Box 451, Princeton, NJ 08544

111. D. R. Mikkelsen, Princeton Plasma Physics Laboratory, P.O. Box 451, Princeton, NJ 08544

112. D. P. Schissel, GA Technologies, Inc., P.O. Box 85608, San Diego, CA 92138

113. P. B. Parks, GA Technologies, Inc., P.O. Box 85608, San Diego, CA 92138

114. P. Gohil, GA Technologies, Inc., P.O. Box 85608, San Diego, CA 92138

115. G. Jackson, GA Technologies, Inc., P.O. Box 85608, San Diego, CA 92138

116. A. D. Cheetham, JET Joint Undertaking, Culham Laboratory, Abingdon, Oxfordshire, OX14 3DB, England

117. A. Gondhalekar, JET Joint Undertaking, Culham Laboratory, Abingdon, Oxfordshire, OX14 3DB, England

118. F. Hendriks, JET Joint Undertaking, Culham Laboratory, Abingdon, Oxfordshire, OX14 3DB, England

119. P. M. Stubberfield, JET Joint Undertaking, Culham Laboratory, Abingdon, Oxfordshire, OX14 3DB, England

120. P. Kupschus, JET Joint Undertaking, Culham Laboratory, Abingdon, Oxfordshire, OX14 3DB, England

121. M. L. Watkins, JET Joint Undertaking, Culham Laboratory, Abingdon, Oxfordshire, OX14 3DB, England

122. K. Kim, University of Illinois, Fusion Studies Laboratory, 214 Nuclear Engineering Laboratory, 103 S. Goodwin Avenue, Urbana, IL 61801

123. G. C. Vlases, University of Washington, Department of Physics, FM-15, Seattle, WA 98195

124. C. T. Chang, Plasma Physics Section, Physics Division, Risø National Laboratory, DK-4000 Roskilde, Denmark

125. H. Sørensen, Plasma Physics Section, Physics Division, RisøNational Laboratory, DK-4000 Roskilde, Denmark

126—241. Given distribution according to TID-4500, Magnetic Fusion Energy (Category Distribution UC-20g, Theoretical Plasma Physics)